

In Situ Growth Strategy to Integrate Up-Conversion Nanoparticles with Ultrasmall CuS for Photothermal Theranostics

Ruichan Lv,^{†,‡,⊥} Piaoping Yang,^{*,‡} Bo Hu,[†] Jiating Xu,[‡] Wenting Shang,[§] and Jie Tian^{*,†,§}

[†]Engineering Research Center of Molecular and Neuro Imaging, Ministry of Education, School of Life Science and Technology, Xidian University, Xi'an, Shanxi 710071, China

[‡]Key Laboratory of Superlight Materials and Surface Technology, Ministry of Education, College of Material Sciences and Chemical Engineering, Harbin Engineering University, Harbin 150001, China

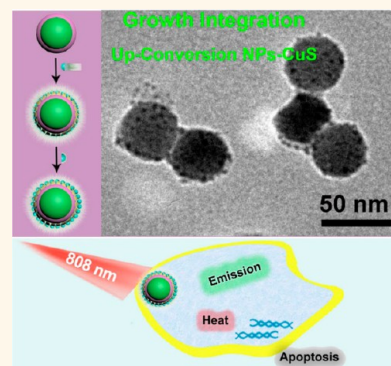
[§]Key Laboratory of Molecular Imaging of Chinese Academy of Sciences, Institute of Automation, Chinese Academy of Sciences, Beijing 100190, China

[⊥]Fachbereich Physik, Philipps Universität Marburg, 35037 Marburg, Germany

Supporting Information

ABSTRACT: In the theranostic field, a near-infrared (NIR) laser is located in the optical window, and up-conversion nanoparticles (UCNPs) could be potentially utilized as the imaging agents with high contrast. Meanwhile, copper sulfide (CuS) has been proposed as a photothermal agent with increased temperature under a NIR laser. However, there is still no direct and effective strategy to integrate the hydrophobic UCNPs with CuS until now. Herein, we propose an *in situ* growth routine based on the hydrophobic core/shell UCNPs combined with ultrasmall water-soluble CuS triggered by single 808 nm NIR irradiation as the theranostic platform. Hydrophobic NaYF₄:Yb,Er@NaYF₄,Nd,Yb could be turned hydrophilic with highly dispersed and biocompatible properties through conjunction with transferred dopamine. The as-synthesized ultrasmall CuS (3 and 7 nm) served as a stable photothermal agent even after several laser-on/off cycles. Most importantly, comparing with the mix routine, the *in situ* growth routine to coat UCNPs with CuS is meaningful, and the platform is uniform and stable. Green luminescence-guided hyperthermia could be achieved under a single 808 nm laser, which was evidenced by *in vitro* and *in vivo* assays. This nanoplatform is applicable as a bioimaging and photothermal antitumor agent, and the *in situ* growth routine could be spread to other integration processes.

KEYWORDS: up-conversion, copper sulfide, *in situ* growth, photothermal



In the theranostic field, a multiple-photon process induced up-conversion luminescence (UCL) produced by near-infrared (NIR) laser irradiation has been proposed as an effective and powerful tool to diagnose and track treatment.^{1–6} Under NIR light irradiation, the absence of laser emission enables UCL nanoparticles to possess enhanced contrast and higher spatial resolution.^{7–14} Thus, NIR-irradiated theranostics has been extensively applied in imaging-guided biological and medical nanotechnology.^{15–23} The most widely used NIR laser locates at a wavelength of 980 nm due to Yb³⁺ ion absorption as sensitizer. Despite many unique advantages for a 980 nm laser, a serious shortcoming still exists because its radiation can be easily absorbed by hemoglobin and water (Figure S1). Consequently, the continuous laser powers absorbed by the tumors and tissues will inevitably transform to heat and produce overheating, thus damaging the normal cells together with cancer cells. Alternatively, Nd³⁺-sensitized UCL materials were recently proposed

using 808 nm light as the irradiation source, which has the high-performance merit to conquer the overheating problem of normal cells and improve the penetration depth.^{24–27}

On the other side, how to transfer hydrophobic UCNPs to hydrophilic ones is still an interesting and essential topic.^{28–30} A dopamine monomer with an aromatic ring and amino and hydroxyl groups could be utilized as the organic precursor.^{31,32} It has been shown that the melanin-like polydopamine can efficiently convert light into heat with excellent biocompatible and biodegradable properties.^{33–35} However, among the traditional photothermal therapy (PTT) agents (such as organic chemicals, metal composites, carbon-based complexes, and semiconductors),^{36–44}

Received: November 29, 2016

Accepted: December 13, 2016

Published: December 13, 2016

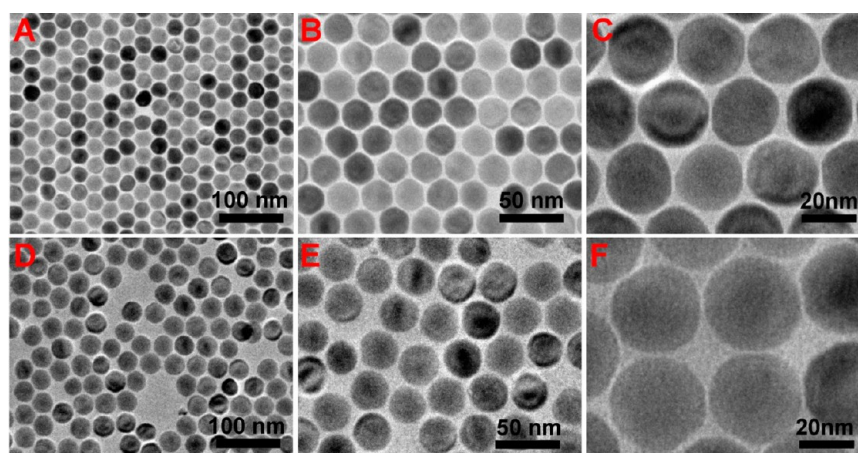


Figure 1. Hydrophobic UCNP. TEM images of (A–C) $\text{NaYF}_4:\text{Yb,Er}$ and (D–F) core/shell $\text{NaYF}_4:\text{Yb,Er}@\text{NaYF}_4:\text{Yb,Nd}$ at different magnifications.

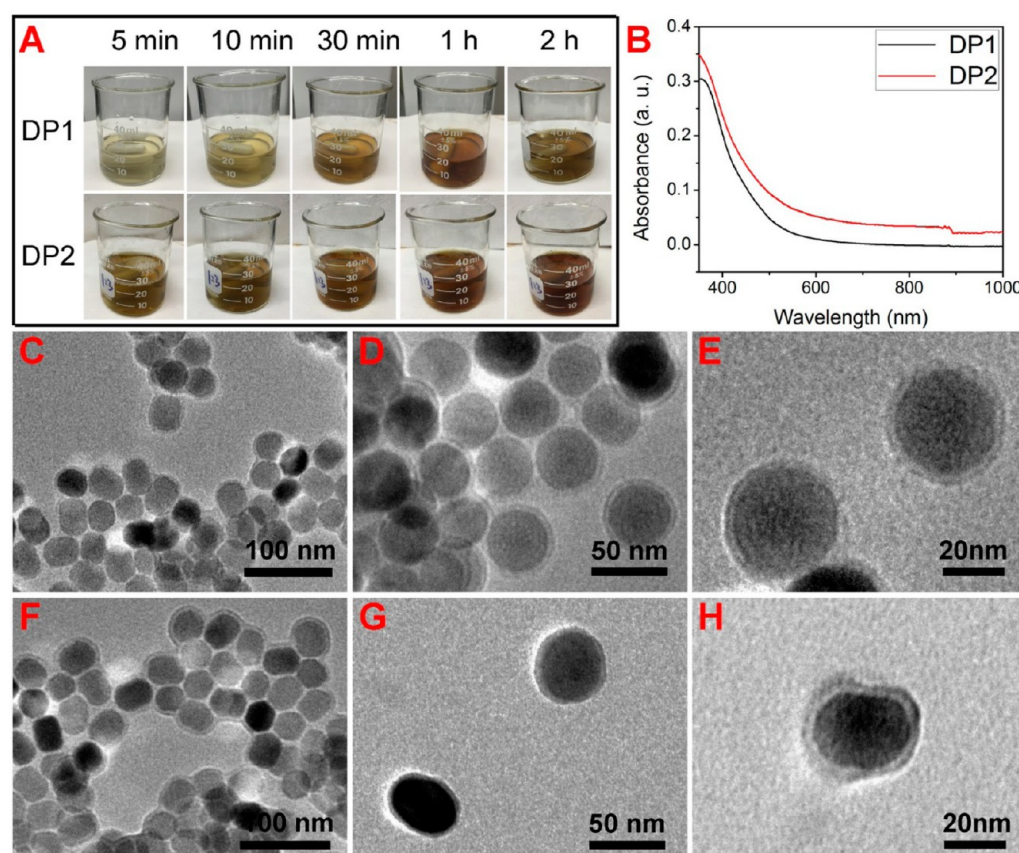


Figure 2. Mix routine of the precursor. (A) Digital photographs and (B) absorbance spectra of transformed dopamine solutions (DP1 and DP2). TEM images at different magnifications of (C–E) UCNP-DP1 and (F–H) UCNP-DP2.

organic compounds have a lower photothermal conversion efficiency and a serious photobleaching effect. Especially, there was no effective way to prevent photobleaching when exposed to irradiation in the body's environment until now.⁴⁵ Meanwhile, for luminescence-guided therapeutic applications, it is beneficial to find agents with a decreased quenching effect from the visible emission.^{46–48} Based on this, NIR-responsive semiconductor nanomaterials with low absorbance in the visible region are promising as theranostic agents together with up-conversion nanoparticles (UCNPs).^{49–51} Especially, copper sulfide (CuS) is long-lasting, low toxic, highly stable, and biodegradable, with no

obvious side effects in the visible emissions.^{51–54} However, until now, there is almost no effective way to integrate hydrophobic UCNPs with the ultrasmall water-soluble CuS directly, because of the inherent difficulty in modifying the UCNPs.

In this research, hydrophobic $\text{NaYF}_4:18\%\text{Yb},2\%\text{Er}@\text{NaYF}_4:30\%\text{Nd},10\%\text{Yb}$ (referred to as $\text{NaYF}_4:\text{Yb,Er}@\text{NaYF}_4:\text{Nd,Yb}$) nanoparticles with green luminescence under 808 nm light irradiation have been synthesized and simply stabilized by transferred dopamine. Ultrasmall CuS nanoparticles (about 3 and 7 nm) were synthesized under a water environment. Two different integration strategies (the mix routine and growth routine) have

been proposed and carried out to obtain UCNPs-CuS with adjustable morphology and UCL intensity. Through combination of the two counterparts, the UCNPs-CuS complex could achieve hyperthermia with green light for photothermal therapy under a single 808 nm laser. The anticancer therapeutic efficiency is verified by the *in vitro* and *in vivo* experiments. This nano-platform is applicable as an NIR theranostic agent, and the growth routine may be applied to other integration processes.

RESULTS AND DISCUSSION

TEM images of $\text{NaYF}_4\text{:Yb,Er}$ nanoparticles as the core are shown in Figure 1A–C. The average size of $\text{NaYF}_4\text{:Yb,Er}$ core nanoparticles is 25 nm. After further epitaxial growth, the size of core/shell $\text{NaYF}_4\text{:Yb,Er@NaYF}_4\text{:Yb,Nd}$ is about 33 nm (Figure 1D–F). The hydrophobic nanoparticles are uniform and well distributed in hexane. Figure S2 shows that the doped lanthanide ions of Y, Yb, and Nd are well distributed in each nanoparticle. The generation process of transferred dopamine solutions (DP1 and DP2) is shown in Figure 2. DP1 and DP2 solutions were synthesized with 0.1 g of polyethylenimine (PEI) and different amounts of dopamine (0.1 and 0.3 g), respectively. With the reaction time increased, the color of the solution changed from colorless to dark, indicating the formation of transferred dopamine (Figure 2A). Meanwhile, when the amount of added PEI molecules increased, the color became darker due to the stronger alkaline condition. UV–vis absorbance spectra indicate there was strong absorbance in the visible region, especially in the region shorter than 500 nm (Figure 2B). When the hydrophobic $\text{NaYF}_4\text{:Yb,Er@NaYF}_4\text{:Yb,Nd}$ was transferred to hydrophilic nanoparticles through modification with DP1 solution and DP2 solution, a pale shell was formed from the nanoparticles (Figure 2C–H), indicating the generation of polydopamine outside of the up-conversion nanoparticles. Compared with the DP1 solution (Figure 2C–E), the pale shell could be increased with a higher amount of PEI-generated transferred dopamine (DP2) solution added (Figure 2F–H). As a comparison, when there is no dopamine added, there is no clear polymer coating on the surface (Figure S3). TEM images of the UCNPs-DP- Cu^{2+} sample are presented in Figure 3, and there is an obvious modified polymer on the surface of the UCNPs. The sample in water solution turned dark green, indicating Cu^{2+} ions were attached on the surface of the UCNPs together with the polydopamine. Figure S4 and Table S1 present the XPS results of

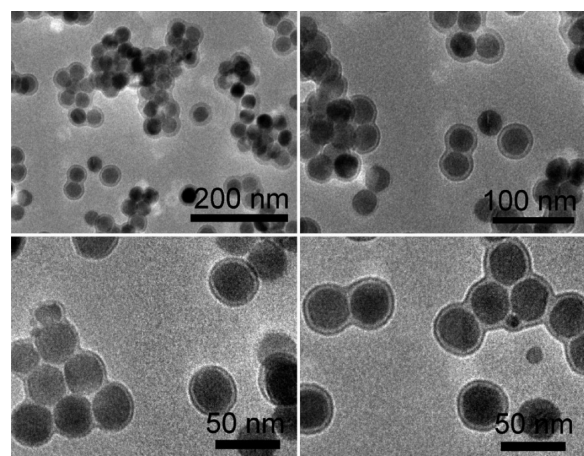


Figure 3. Growth routine of the precursor. TEM images at different magnifications of UCNPs-DP- Cu^{2+} .

the as-prepared UCNPs-DP- Cu^{2+} and the Na^+ , F^- , Y^{3+} , Yb^{3+} , Nd^{3+} , and Cu^{2+} ions, respectively.

Although the synthesis process of different water-soluble CuS samples is similar, the samples could be different with the reaction ratios and reaction times changed. TEM images of CuS with different reaction conditions (reaction ratios of Cu-Cit: Na_2S varied from 4:1 to 1:2) are shown in Figure 4A,B. As shown, the two samples are well dispersed, with an average size of 3 nm (ratio of 1:1 for 15 min) and 7 nm (ratio of 1:2 for 5 min), respectively. The absorbance spectra of CuS with different reaction conditions (Figure 4C,D) indicate that decreased absorbance in the NIR region (around 800 nm) occurs when the amount of Na_2S is increased. When the reactant ratio is 2:1, there was almost no change as the time increased from 15 min to 30 min (Figure S5). Thus, we took 15 min as the end time of the reaction. The reaction processes were similar when the reactant ratio was 4:1, 2:1, and 1:1. However, during the reaction process, the color of the solution changed from light blue to deep green on prolonging the reaction time when the reactant ratio was 1:2. The precipitate was generated easily when stirring continued for 15 min, and this is the reason that the absorbance intensity in the visible region enhanced drastically. TEM images of the precipitation are shown in Figure S6. The micropowders are composed of nanospheres, indicating the copper sulfide micropowders are generated with the aggregation of nanoparticles.

From the absorbance spectra, we can see both of the CuS nanoparticles have a wide band gap absorption with a blue-shifted property compared with bulk CuS materials (with the peak wavelength higher than 1100 nm), indicating a quantum size confinement. On the basis of the extinction coefficient equation $\epsilon = \pi^2/6d^3FN_{\text{A}}LC_{\text{wt}}$, the extinction coefficient increases accordingly when the average size (d) of CuS is decreased and the absorbance (A) value is increased. Compared with the reported literature, the absorption peak was blue-shifted to ~ 800 nm.⁵⁵ After 808 nm irradiation (laser power: 0.7 W) for 5 min, the temperature of the two solutions (concentration: 1 mg mL^{-1}) could be gradually increased to 48.3 and 42.3 $^{\circ}\text{C}$, respectively (Figure 4E,F). More importantly, after further turning on and off for 5 min, the maximum temperature of the first CuS sample (reaction ratio of 1:1 for 15 min) remained stable (48.3 to 49.9 $^{\circ}\text{C}$) after several laser-on/off cycles (more than 6 cycles in 1 h), while the second sample (reaction ratio of 1:2 for 5 min) decreased a little (42.3 to 41.5 $^{\circ}\text{C}$). That means the CuS sample with the reaction ratio of 1:1 for 15 min has an outstanding stability.

Two routines (mix and growth) were carried out to integrate UCNPs with CuS. After combination by the mix routine, the hydrophilic composite is well-dispersed in the water solution with an average size of 150 nm (Figure 5A). As shown in Figure 5B and C, UCNPs are surrounded by dense ultrasmall CuS nanoparticles. Note that the combination procedure should be processed with the assistance of DP2 solution (2 mL), to promote the conjunction between the $-\text{COOH}$ group in CuS and the $-\text{NH}_2$ group in UCNPs. Without DP2 solution added, it is difficult to combine the ultrasmall CuS nanoparticles into UCNPs (Figure S7).

TEM images of UCNPs-CuS synthesized by the *in situ* growth routine are presented in Figure 5D–F and Figure S8. Alternatively, the water-soluble ultrasmall CuS nanoparticles are well conjugated on the surface of UCNPs. Most importantly, the uniform UCNPs synthesized by the growth routine keep a similar size (less than 50 nm) to the initial hydrophilic ones, indicating a potential application as a theranostic agent. Also, in

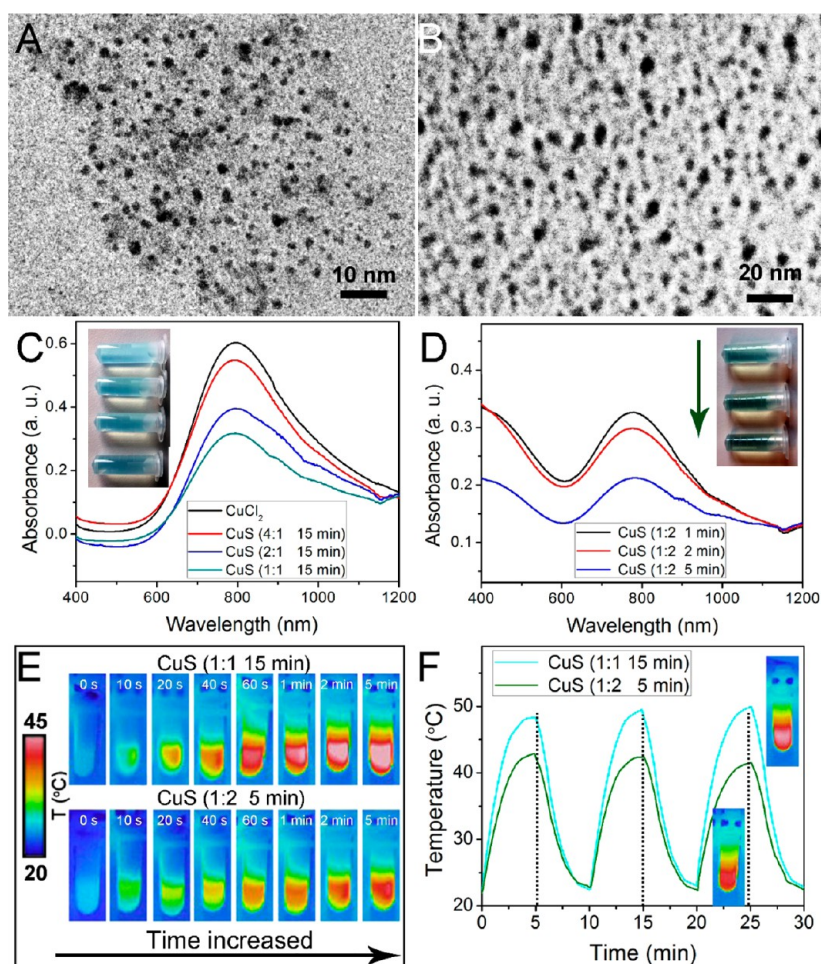


Figure 4. Properties of CuS. (A, B) TEM images and (C, D) absorbance spectra of CuS solutions with different reaction conditions. (E) Thermal imaging and (F) temperature change curves of CuS solutions with different conditions under 808 nm NIR light irradiation.

the HRTEM image (Figure 5G), two main lattice distances of 0.52 and 0.30 nm correspond to the (100) plane of NaYF₄ and the (102) lattice of CuS, respectively. After detection by ICP-MS, the ratio of Y, Yb, and Cu elements in UCNP-CuS was 63:30:9. As shown in Figure S9, there are Na, Y, Yb, Nd, F, and Cu in this structure. Note that the Si element is due to the silica plate (sample carrier). Also, there is an obvious increased absorbance of the UCNP-CuS in the NIR region (600–1000 nm) compared with the UCNP solution due to the combination of CuS nanoparticles (Figure 5H).

The as-synthesized hydrophobic NaYF₄:Yb,Er@NaYF₄:Yb,Nd in hexane could emit bright green light under 808 nm irradiation even in daylight (Figure S10). High up-conversion intensity of this structure could be used as a promising diagnose probe. Two main emissions in the green regions (521 nm, 540 nm) and red regions (654 nm) correspond to $^2\text{H}_{11/2}/^4\text{S}_{3/2} \rightarrow ^4\text{I}_{15/2}$ and $^4\text{F}_{9/2} \rightarrow ^4\text{I}_{15/2}$ up-conversion processes, respectively. The two samples after integration with CuS using different routines in water could emit bright green light under daylight (inset of Figure 5I). Meanwhile, the UCNP-CuS (growth) has brighter green light than UCNP-CuS (mix) due to the decreased absorption (thinner coated CuS shell) of the laser excitation, indicating the emission intensity could be adjusted by the loading amount of CuS (Figure 5I).

The inverted fluorescence microscope images of MCF-7 cells incubated with UCNP-CuS are shown in Figure 6A. As shown,

the samples could be well intracellular and emit bright green light under 808 nm irradiation. The biocompatibility property of UCNP-CuS was necessary for further bioapplication. The as-synthesized UCNP-CuS could be well dispersed into different physiological solutions, such as PBS and medium including serum (Figure S11A). Meanwhile, the UV-vis-NIR spectra of UCNP-CuS in water and PBS are similar, indicating that UCNP-CuS have no side effects or reactions in different biosolutions (Figure S11B). Furthermore, the viability of cells when incubated with UCNP-CuS was detected using an MTT assay. The viability of L929 cells at concentrations of 15.6–500 $\mu\text{g}/\text{mL}$ is 92.9–107.1% (Figure 6B), indicating the as-prepared material has no side effects on normal cells. The photograph and infrared thermal images of MCF-7 cells in a 96-well plate incubated with UCNP-CuS are presented in Figure 6C, and the temperature of the culture with UCNP-CuS added could be increased highly (51.4 °C) under 808 nm irradiation (0.72 W/cm²). The high temperature is able to kill cancer cells effectively. Then, the anticancer efficiency of UCNP-CuS under 808 nm irradiation was detected. As shown in Figure 6D, the CuS group (viability of 34.8% with the highest concentration of 500 $\mu\text{g}/\text{mL}$) and UCNP-CuS group (viability of 38.7% with the highest concentration of 500 $\mu\text{g}/\text{mL}$) of the same CuS concentrations have similar viability under 808 nm irradiation. The live/dead state of cancer cells with intracellular UCNP-CuS before and after 808 nm laser irradiation was

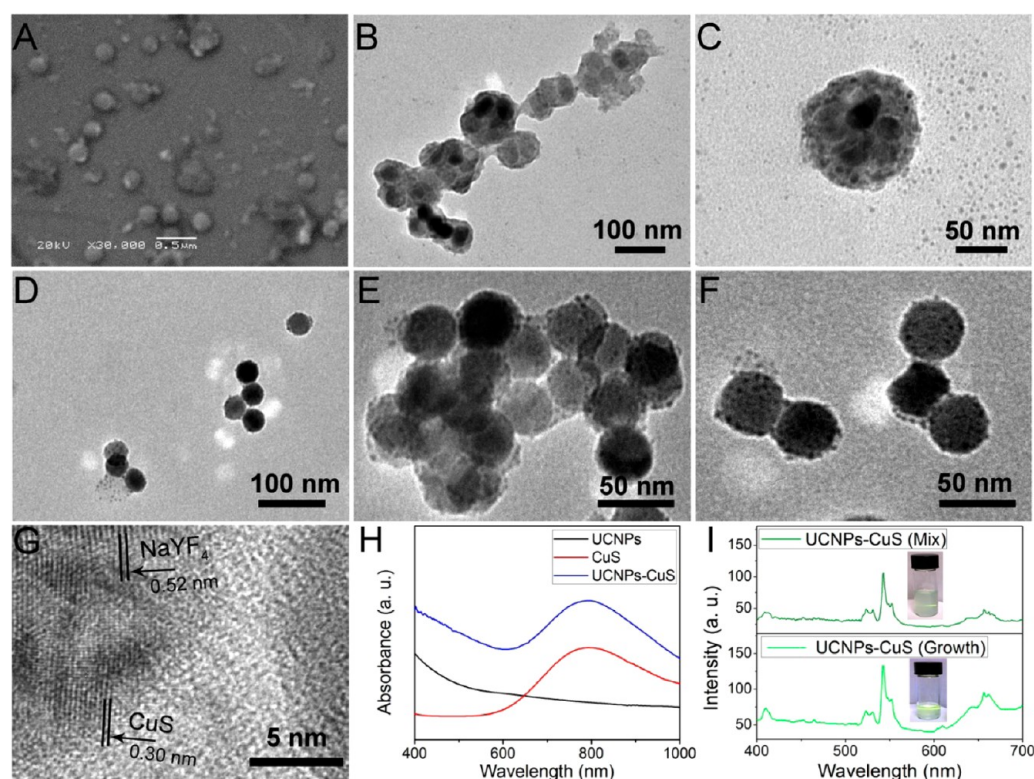


Figure 5. Properties of UCNPs-CuS. SEM and TEM images with different magnifications of (A–C) UCNPs-CuS (mix) and (D–F) UCNPs-CuS (growth). (G) HRTEM image of UCNPs-CuS. (H) Absorbance spectra of UCNPs, CuS, and UCNPs-CuS solutions. (I) UCL emission spectra of UCNPs-CuS solutions with different integration strategies.

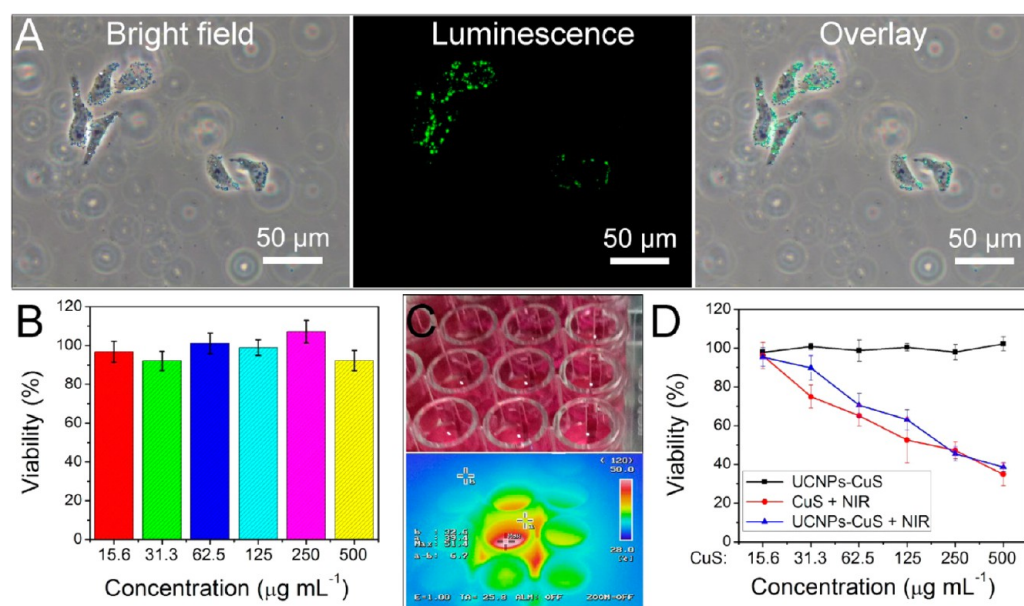


Figure 6. *In vitro* imaging-guided photothermal therapy. (A) Inverted fluorescence microscope images of MCF-7 cells incubated with UCNPs-CuS upon 808 nm NIR light irradiation. (B) Cell viability of UCNPs-CuS incubated with the L929 cell line using the MTT assay. (C) Digital photograph and infrared thermal image of MCF-7 cells in a 96-well plate incubated with UCNPs-CuS under 808 nm NIR laser irradiation. (D) *In vitro* anticancer efficiency of UCNPs-CuS, CuS under 808 nm laser irradiation and UCNPs-CuS under 808 nm laser irradiation.

detected with Calcein AM and propidium iodide (PI) staining (Figure S12). Compared with the control group without laser irradiation, the cells were almost killed under 808 nm irradiation.

For potential application in the clinical field, it is essential to detect the *in vivo* biocompatibility and anticancer therapeutic effect. Figure S13A shows the pharmacokinetics of the blood

circulation curve. The fitted curve presents a two-component model with first-phase and second-phase blood circulation half-lives at 0.054 ± 0.099 day and 0.535 ± 0.106 day, respectively. As shown in Figure S13B, in the early stages (10 min and 1, 4, and 12 h after injection), the nanoparticles accumulated in the liver and spleen. In the whole detection time, Y concentrations

remained low in the heart and kidney. Y concentrations were reduced in the liver, spleen, and lung after 24 h. On the seventh and 14th day, the nanoparticles in the liver, spleen, and lung are much less than on 1 day. The results reveal that the injected UCNPs-CuS could be excreted from the mice.

The *in vivo* theranostics results of UCNPs-CuS are shown in Figure S14. After being treated with different conditions every 2 days for 14 days, the mice and tumors from different groups (the blank group, the groups with 808 nm laser, and UCNPs-CuS with 808 nm laser) were examined. The third group shows the highest tumor inhibition effect, while the 808 nm laser has a negligible effect on the tumors (Figure S14A and C). Figure 14B shows that the UCNPs-CuS could emit green light under 808 nm irradiation. The photo inset of Figure S11B was obtained with a filter inserted. Meanwhile, the body weights keep increasing (Figure S14D), revealing that there are no side effects of UCNPs-CuS. H&E-stained images of liver and kidney from different groups showed that no damage is found in the hepatocytes and no concentration is observed in the glomerulus (Figure S14E). All the *in vitro* and *in vivo* results evidently demonstrate that UCNPs-CuS could be well utilized as a potential photothermal theranostic agent.

CONCLUSIONS

In sum, hydrophilic core/shell up-conversion nanoparticles have been synthesized and coated with transferred dopamine. Compared with the mix routine, the *in situ* growth routine to coat CuS on the UCNPs is meaningful and the platform is uniform and stable. Green luminescence-guided hyperthermia could be achieved induced by a single 808 nm laser and was evidenced by *in vitro* and *in vivo* assays. This nanoplatform can be applicable as a bioimaging agent and effective antitumor agent for theranostics, and the growth routine could be applied to other integration processes.

EXPERIMENTAL SECTION

Reagents and Materials. All chemical reagents used are analytical grade without any further purification. $\text{Y}(\text{CH}_3\text{COO})_3$ (99.9%), $\text{Yb}(\text{CH}_3\text{COO})_3$ (99.9%), $\text{Er}(\text{CH}_3\text{COO})_3$ (99.9%), Y_2O_3 (99.99%), Nd_2O_3 (99.99%), and Yb_2O_3 (99.99%) were obtained from Sinopharm Chemical Reagent Co., Ltd., Shanghai, China. Cyclohexane, phosphate-buffered saline (PBS), glutaraldehyde, and dimethyl sulfoxide (DMSO) were obtained from Tianjin Kermel Chemical Reagent Co., Ltd., Tianjin, China. Oleic acid (OA, technical grade), 1-octadecene (ODE, technical grade), trifluoroacetic acid (CF_3COOH , 99%), copper chloride (CuCl_2), sodium sulfide (Na_2S), polyethylenimine (MW = 25000), sodium citrate (Na_3Cit), glycerol, MTT (3-(4,5-dimethylthiazol-2-yl)-2,5-diphenyltetrazolium bromide), Calcein AM, and propidium iodide were purchased from Sigma-Aldrich, China. Polyethylene glycol (PEG500) and sodium trifluoroacetate (CF_3COONa , 98%) were purchased from Beijing Chemical Corporation, Beijing, China.

Synthesis of $\text{NaYF}_4\text{:18\%Yb,2\%Er}$. The syntheses were carried out according to the reported literature with little modification.⁵⁶ Typically, lanthanide precursors of $\text{Ln}(\text{CH}_3\text{COO})_3$ (Ln = 80% Y, 18% Yb, and 2% Er) were mixed in a three-necked bottle with 9 mL of oleic acid and 15 mL of octadecene. The mixture was heated to 160 °C under an argon atmosphere and kept for 1 h to obtain a clear solution (solution A). Then, 4 mmol of NH_4F and 2.5 mmol of NaOH were mixed and sonicated for 10 min (solution B). After solution A was cooled to room temperature, solution B was injected directly and stirred for 30 min. After that, the mixed solution was heated to 100 °C and kept for another 20 min. Then, the solution was heated to 300 °C and kept for 1 h. Finally, the solution was washed and centrifuged with ethanol to obtain the $\text{NaYF}_4\text{:18\%Yb,2\%Er}$ nanoparticles. After drying in the air, the precipitate was obtained and dissolved in hexane.

Synthesis of Core/Shell $\text{NaYF}_4\text{:18\%Yb,2\%Er@NaYF}_4\text{:30\%Yb,10\%Nd}$. $\text{Ln}(\text{CF}_3\text{COO})_3$ (Ln = 60% Y, 30% Nd, and 10% Yb) was mixed with $\text{NaYF}_4\text{:18\%Yb,2\%Er}$, and 9 mL of oleic acid and 15 mL of octadecene were added. After stirring at 120 °C under an argon atmosphere, the clear solution was heated and kept at 310 °C for another 30 min. Finally, the solution was washed and centrifuged with ethanol to obtain the nanoparticles. After drying in air, the precipitate of $\text{NaYF}_4\text{:18\%Yb,2\%Er@NaYF}_4\text{:30\%Yb,10\%Nd}$ was obtained and dissolved in hexane.

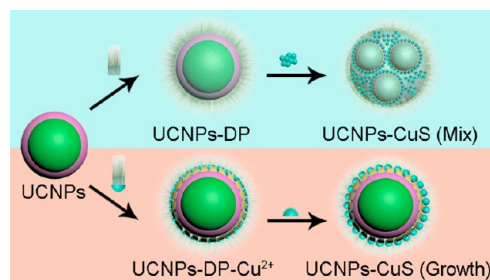
Synthesis of Hydrophilic UCNPs-DP1 and UCNPs-DP2. Hydrophilic UCNPs were transferred from $\text{NaYF}_4\text{:18\%Yb,2\%Er@NaYF}_4\text{:30\%Yb,10\%Nd}$ with the transferred dopamine (DP1 and DP2). DP1 solution was synthesized with 0.1 g of PEI and 0.1 g of dopamine mixed into 20 mL of deionized water for 2 h, and DP2 solution was synthesized with 0.3 g of PEI and 0.1 g of dopamine mixed into 20 mL of deionized water for 2 h, respectively. The mixture was stirred for 12 h, and the obtained solution was labeled as DP1 or DP2. Then, the DP1 or DP2 solution was mixed with 0.2 mM of the as-synthesized core/shell nanoparticles separately. After further stirring for 12 h in an open beaker under room temperature, the solution was centrifuged and the brown precipitate was labeled as hydrophilic UCNPs-DP1 or UCNPs-DP2.

Synthesis of UCNPs-CuS by the Mix Routine. Different CuS nanoparticles are obtained using deionized water as the reaction environment. The CuCl_2 (1 mmol) and Na_3Cit (0.02 g) were first mixed into 1 mL of water to get a blue solution (solution I), and then Na_2S (0.02 g) was dissolved into 1 mL of water (solution II). Different particles are generated with adjusted reactant ratios (solution I:solution II) added into 30 mL of deionized water; note that the CuCl_2 and Na_3Cit were added first, and the Na_2S solution was added drop by drop. After the reactant was mixed and stirred under room temperature for 5 min, the solution was kept at 90 °C for 15 min. After that, the solution was put into ice water and kept cold for further use.

For UCNPs-CuS (mix), the hydrophilic UCNPs were dissolved in 30 mL of the as-synthesized CuS solution; then 5 mL of DP solution was added simultaneously for better combination of the two composites. After stirring for 4 h, the UCNPs-CuS was obtained by centrifugation and washed with deionized water.

Synthesis of Hydrophilic UCNPs-CuS by the Growth Routine. Another way to make hydrophobic UCNPs hydrophilic is carried out with little change. During the transferring process from UCNPs to UCNPs-DP1 or UCNPs-DP2, 1 mM of $\text{CuCl}_2\cdot 2\text{H}_2\text{O}$ was added simultaneously; then, after 12 h of stirring, the as-synthesized powders were labeled as UCNPs-DP-Cu²⁺. Then, 0.01 g of Na_3Cit and 0.01 g of Na_2S were added and reacted according to the CuS synthesis process. The final dark green powders were labeled as UCNPs-CuS (growth) and applied as a photothermal theranostic agent. A schematic diagram of the two synthesis processes is shown in Scheme 1. Compared with the mix

Scheme 1. Schematic Diagram of Different Integration Strategies (Mix and Growth Routines) of UCNPs-CuS



routine, the Cu^{2+} ions in the growth routine could be introduced before the CuS was generated, which could be used to control the final position of CuS nanoparticles on the surface of the UCNPs.

Characterization. Morphology images were obtained digitally on a scanning electron microscope (SEM, JSM-6480A) and a transmission electron microscopy (TEM, FEI Tecnai G² S-Twin). The X-ray photoelectron spectrum (XPS) was measured on an AXIS ULTRADL

(Kratos) using an Al target as the X-ray source. UCL emission spectra were obtained on an Edinburgh FLS 980 using an 808 nm laser diode controller as separate laser sources. The absorbance spectra of the solutions were recorded on a UV-1601 spectrophotometer. Confocal laser scanning microscopy images were recorded using a Leica SP2.

In Vitro Cellular Uptake. The cellular uptake process was studied using MCF-7 cells. Briefly, the cells were cultured to get a monolayer in the six-well plates with coverslips. Then, the cells were incubated with UCNPs-CuS at 37 °C for 3 h. After that, the well was washed with 1 mL of 2.5% glutaraldehyde for fixation for 10 min. After further washing with PBS, the coverslip was recoded on a Nikon Ti-S with external 980 nm laser irradiation.

In Vitro Biocompatibility Using the MTT Assay. Typically, L929 cells were put in a 96-well plate (about 6000 per well) to obtain a monolayer, and then materials with different concentrations (500, 250, 125, 62.5, 31.3, and 15.6 $\mu\text{g mL}^{-1}$) were added. The blank well without material added was considered as the control. After incubating for another 24 h, 20 μL of MTT solution (5 mg mL^{-1}) was added to each well and incubated for another 4 h. Then, the mixture was discarded, and DMSO (150 μL) solvent was added to dissolve the produced formazan. Finally, the plate was put on the microplate reader, and the absorbance values were recorded at the wavelength of 490 nm.

In Vitro Anticancer Efficiency Using the MTT Assay. The anticancer therapy efficiency was detected on the MCF-7 cell lines. First, cancer cells were put in a 96-well plate (about 6000 per well) to obtain a monolayer, and then UCNPs-CuS and CuS nanoparticles with different concentrations (500, 250, 125, 62.5, 31.3, and 15.6 $\mu\text{g mL}^{-1}$) were added. After incubating for another 24 h, 20 μL of MTT solution (5 mg mL^{-1}) was added to each well and incubated for another 4 h. Then, the mixture was discarded, and 150 μL of DMSO solvent was added to dissolve the produced formazan. Finally, the plate was put on the microplate reader, and the absorbance values were recorded at the wavelength of 490 nm.

ASSOCIATED CONTENT

Supporting Information

The Supporting Information is available free of charge on the ACS Publications website at DOI: 10.1021/acsnano.6b07990.

In vivo experimental details; photographs; and spectra (PDF)

AUTHOR INFORMATION

Corresponding Authors

*E-mail: yangpiaoping@hrbeu.edu.cn.

*E-mail: jie.tian@ia.ac.cn.

ORCID

Ruichan Lv: 0000-0002-6360-6478

Notes

The authors declare no competing financial interest.

ACKNOWLEDGMENTS

Financial support from the Natural Science Foundation of China (NSFC 21271053, 21401032, 51472058, 51332008, 51502050) is greatly acknowledged. We thank Ziyao Liu, Mahmoud G. Soliman, and Indranath Chakraborty in Wolfgang J. Parak's group for related cell experiments, SEM mapping, and ICP-MS analysis, respectively. R.L. acknowledges the postdoctoral fellowship from the Alexander von Humboldt Foundation.

REFERENCES

(1) Dai, Y.; Xiao, H.; Liu, J.; Yuan, Q.; Ma, P. a.; Yang, D.; Li, C.; Cheng, Z.; Hou, Z.; Yang, P.; Lin, J. *In Vivo* Multimodality Imaging and Cancer Therapy by Near-Infrared Light-Triggered trans-Platinum Pro-Drug-Conjugated Upconversion Nanoparticles. *J. Am. Chem. Soc.* **2013**, *135*, 18920–18929.

(2) Zeng, S.; Yi, Z.; Lu, W.; Qian, C.; Wang, H.; Rao, L.; Zeng, T.; Liu, H.; Liu, H.; Fei, B.; Hao, J. Simultaneous Realization of Phase/Size Manipulation, Upconversion Luminescence Enhancement, and Blood Vessel Imaging in Multifunctional Nanoprobes Through Transition Metal Mn^{2+} Doping. *Adv. Funct. Mater.* **2014**, *24*, 4051–4059.

(3) Ostrowski, A. D.; Chan, E. M.; Gargas, D. J.; Katz, E. M.; Han, G.; Schuck, P. J.; Milliron, D. J.; Cohen, B. E. Controlled Synthesis and Single-Particle Imaging of Bright, Sub-10 nm Lanthanide-Doped Upconverting Nanocrystals. *ACS Nano* **2012**, *6*, 2686–2692.

(4) Zheng, W.; Huang, P.; Tu, D.; Ma, E.; Zhu, H.; Chen, X. Lanthanide-Doped Upconversion Nano-Bioprobe: Electronic Structures, Optical Properties, and Biodetection. *Chem. Soc. Rev.* **2015**, *44*, 1379–1415.

(5) Liu, X.; Yan, C.-H.; Capobianco, J. A. Photon Upconversion Nanomaterials. *Chem. Soc. Rev.* **2015**, *44*, 1299–1301.

(6) Li, Y.; Tang, J.; Pan, D.-X.; Sun, L.-D.; Chen, C.; Liu, Y.; Wang, Y.-F.; Shi, S.; Yan, C.-H. A Versatile Imaging and Therapeutic Platform Based on Dual-Band Luminescent Lanthanide Nanoparticles toward Tumor Metastasis Inhibition. *ACS Nano* **2016**, *10*, 2766–2773.

(7) Zhou, J.; Liu, Q.; Feng, W.; Sun, Y.; Li, F. Upconversion Luminescent Materials: Advances and Applications. *Chem. Rev.* **2015**, *115*, 395–465.

(8) Chen, G.; Roy, I.; Yang, C.; Prasad, P. N. Nanochemistry and Nanomedicine for Nanoparticle-based Diagnostics and Therapy. *Chem. Rev.* **2016**, *116*, 2826–2885.

(9) Heer, S.; Kompe, K.; Gudel, H. U.; Haase, M. Highly Efficient Multicolour Upconversion Emission in Transparent Colloids of Lanthanide-Doped NaYF_4 Nanocrystals. *Adv. Mater.* **2004**, *16*, 2102–2105.

(10) Shen, J.; Chen, G.; Ohulchanskyy, T. Y.; Kesseli, S. J.; Buchholz, S.; Li, Z.; Prasad, P. N.; Han, G. Tunable Near Infrared to Ultraviolet Upconversion Luminescence Enhancement in $(\alpha\text{-NaYF}_4\text{:Yb,Tm})/\text{CaF}_2$ Core/Shell Nanoparticles for *In situ* Real-time Recorded Biocompatible Photoactivation. *Small* **2013**, *9*, 3213–3217.

(11) Zhao, J.; Jin, D.; Schartner, E. P.; Lu, Y.; Liu, Y.; Zvyagin, A. V.; Zhang, L.; Dawes, J. M.; Xi, P.; Piper, J. A.; Goldys, E. M.; Monro, T. M. Single-Nanocrystal Sensitivity Achieved by Enhanced Upconversion Luminescence. *Nat. Nanotechnol.* **2013**, *8*, 729–734.

(12) Yang, Y.; Liu, J.; Sun, X.; Feng, L.; Zhu, W.; Liu, Z.; Chen, M. Near-Infrared Light-Activated Cancer Cell Targeting and Drug Delivery with Aptamer-Modified Nanostructures. *Nano Res.* **2016**, *9*, 139–148.

(13) Wang, G.; Peng, Q.; Li, Y. Lanthanide-Doped Nanocrystals: Synthesis, Optical-Magnetic Properties, and Applications. *Acc. Chem. Res.* **2011**, *44*, 322–332.

(14) Wen, H.; Zhu, H.; Chen, X.; Hung, T. F.; Wang, B.; Zhu, G.; Yu, S. F.; Wang, F. Upconverting Near-Infrared Light Through Energy Management in Core-Shell Nanoparticles. *Angew. Chem., Int. Ed.* **2013**, *52*, 13419–13423.

(15) Liu, J.; Bu, W.; Pan, L.; Shi, J. NIR-Triggered Anticancer Drug Delivery by Upconverting Nanoparticles with Integrated Azobenzene-Modified Mesoporous Silica. *Angew. Chem., Int. Ed.* **2013**, *52*, 4375–4379.

(16) Lin, H.; Yu, T.; Tsang, M.-K.; Bai, G.; Zhang, Q.; Hao, J. Near-Infrared-to-Near-Infrared Down-Shifting and Upconversion Luminescence of KY_3F_{10} with Single Dopant of Nd^{3+} Ion. *Appl. Phys. Lett.* **2016**, *108*, 041902.

(17) Carlos, L. D.; Ferreira, R. A. S.; Bermudez, V. d. Z.; Julian-Lopez, B.; Escribano, P. Progress on Lanthanide-Based Organic-Inorganic Hybrid Phosphors. *Chem. Soc. Rev.* **2011**, *40*, 536–549.

(18) Gorris, H. H.; Wolfbeis, O. S. Photon-Upconverting Nanoparticles for Optical Encoding and Multiplexing of Cells, Biomolecules, and Microspheres. *Angew. Chem., Int. Ed.* **2013**, *52*, 3584–3600.

(19) Zeng, S.; Wang, H.; Lu, W.; Yi, Z.; Rao, L.; Liu, H.; Hao, J. Dual-modal Upconversion Fluorescent/X-Ray Imaging using Ligand-Free Hexagonal Phase $\text{NaLuF}_4\text{:Gd/Yb/Er}$ Nanorods for Blood Vessel Visualization. *Biomaterials* **2014**, *35*, 2934–2941.

(20) Wang, C.; Tao, H.; Cheng, L.; Liu, Z. Near-infrared Light Induced *in Vivo* Photodynamic Therapy of cancer Based on Upconversion Nanoparticles. *Biomaterials* **2011**, *32*, 6145–6154.

- (21) Wang, Y.; Song, S.; Liu, J.; Liu, D.; Zhang, H. ZnO-Functionalized Upconverting Nanotheranostic Agent: Multi-Modality Imaging-Guided Chemotherapy with On-Demand Drug Release Triggered by pH. *Angew. Chem., Int. Ed.* **2015**, *54*, 536–540.
- (22) Garcia, J. V.; Yang, J.; Shen, D.; Yao, C.; Li, X.; Wang, R.; Stucky, G. D.; Zhao, D.; Ford, P. C.; Zhang, F. NIR-Triggered Release of Caged Nitric Oxide using Upconverting Nanostructured Materials. *Small* **2012**, *8*, 3800–3805.
- (23) Jayakumar, M. K. G.; Bansal, A.; Huang, K.; Yao, R.; Li, B. N.; Zhang, Y. Near-Infrared-Light-Based NanoPlatform Boosts Endosomal Escape and Controls Gene Knockdown *in Vivo*. *ACS Nano* **2014**, *8*, 4848–4858.
- (24) Xie, X.; Gao, N.; Deng, R.; Sun, Q.; Xu, Q.-H.; Liu, X. Mechanistic Investigation of Photon Upconversion in Nd³⁺-Sensitized Core-Shell Nanoparticles. *J. Am. Chem. Soc.* **2013**, *135*, 12608–12611.
- (25) Wang, Y.-F.; Liu, G.-Y.; Sun, L.-D.; Xiao, J.-W.; Zhou, J.-C.; Yan, C.-H. Nd³⁺-Sensitized Upconversion Nanophosphors: Efficient *in Vivo* Bioimaging Probes with Minimized Heating Effect. *ACS Nano* **2013**, *7*, 7200–7206.
- (26) Wang, D.; Xue, B.; Kong, X.; Tu, L.; Liu, X.; Zhang, Y.; Chang, Y.; Luo, Y.; Zhao, H.; Zhang, H. 808 nm Driven Nd³⁺-Sensitized Upconversion Nanostructures for Photodynamic Therapy and Simultaneous Fluorescence imaging. *Nanoscale* **2015**, *7*, 190–197.
- (27) Ai, X. Z.; Ho, C. J. H.; Aw, J.; Attia, A. B. E.; Mu, J.; Wang, Y.; Wang, X. Y.; Wang, Y.; Liu, X. G.; Chen, H. B.; Gao, M. Y.; Chen, X. Y.; Yeow, E. K. L.; Liu, G.; Olivo, M.; Xing, B. G. *In Vivo* Covalent Cross-Linking of Photon-Converted Rare-Earth Nanostructures for Tumour Localization and Theranostics. *Nat. Commun.* **2016**, *7*, 1043210.1038/ncomms10432
- (28) Li, R.; Ji, Z.; Dong, J.; Chang, C. H.; Wang, X.; Sun, B.; Wang, M.; Liao, Y.-P.; Zink, J. I.; Nel, A. E.; Xia, T. Enhancing the Imaging and Biosafety of Upconversion Nanoparticles through Phosphonate Coating. *ACS Nano* **2015**, *9*, 3293–3306.
- (29) Yin, Z. F.; Wu, L.; Yang, H. G.; Su, Y. H. Recent Progress in Biomedical Applications of Titanium Dioxide. *Phys. Chem. Chem. Phys.* **2013**, *15*, 4844–4858.
- (30) Sun, Y.; Feng, W.; Yang, P.; Huang, C.; Li, F. The Biosafety Of Lanthanide Upconversion Nanomaterials. *Chem. Soc. Rev.* **2015**, *44*, 1509–1525.
- (31) Ling, D.; Park, W.; Park, Y. I.; Lee, N.; Li, F.; Song, C.; Yang, S.-G.; Choi, S. H.; Na, K.; Hyeon, T. Multiple-Interaction Ligands Inspired by Mussel Adhesive Protein: Synthesis of Highly Stable and Biocompatible Nanoparticles. *Angew. Chem., Int. Ed.* **2011**, *50*, 11360–11365.
- (32) Lin, L.-S.; Cong, Z.-X.; Cao, J.-B.; Ke, K.-M.; Peng, Q.-L.; Gao, J.; Yang, H.-H.; Liu, G.; Chen, X. Multifunctional Fe₃O₄@Polydopamine Core-Shell Nanocomposites for Intracellular mRNA Detection and Imaging-Guided Photothermal Therapy. *ACS Nano* **2014**, *8*, 3876–3883.
- (33) Zeng, Y.; Zhang, D.; Wu, M.; Liu, Y.; Zhang, X.; Li, L.; Li, Z.; Han, X.; Wei, X.; Liu, X. Lipid-AuNPs@PDA Nanohybrid for MRI/CT Imaging and Photothermal Therapy of Hepatocellular Carcinoma. *ACS Appl. Mater. Interfaces* **2014**, *6*, 14266–14277.
- (34) Kumar, A.; Kumar, S.; Rhim, W.-K.; Kim, G.-H.; Nam, J.-M. Oxidative Nanopeeling Chemistry-Based Synthesis and Photodynamic and Photothermal Therapeutic Applications of Plasmonic Core-Petal Nanostructures. *J. Am. Chem. Soc.* **2014**, *136*, 16317–16325.
- (35) Black, K. C. L.; Yi, J.; Rivera, J. G.; Zelasko-Leon, D. C.; Messersmith, P. B. Polydopamine-Enabled Surface Functionalization of Gold Nanorods for Cancer Cell-Targeted Imaging and Photothermal Therapy. *Nanomedicine* **2013**, *8*, 17–28.
- (36) Song, X. R.; Wang, X. Y.; Yu, S. X.; Cao, J. B.; Li, S. H.; Li, J.; Liu, G.; Yang, H. H.; Chen, X. Y. Co₉Se₈ Nanoplates as a New Theranostic Platform for Photoacoustic/Magnetic Resonance Dual-Modal-Imaging-Guided Chemo-Photothermal Combination Therapy. *Adv. Mater.* **2015**, *27*, 3285–3291.
- (37) Antaris, A. L.; Robinson, J. T.; Yaghi, O. K.; Hong, G.; Diao, S.; Luong, R.; Dai, H. Ultra-Low Doses of Chirality Sorted (6,5) Carbon Nanotubes for Simultaneous Tumor Imaging and Photothermal Therapy. *ACS Nano* **2013**, *7*, 3644–3652.
- (38) Zhu, X.; Feng, W.; Chang, J.; Tan, Y.-W.; Li, J.; Chen, M.; Sun, Y.; Li, F. Temperature-Feedback Upconversion Nanocomposite for Accurate Photothermal Therapy at Facile Temperature. *Nat. Commun.* **2016**, *7*, 1043710.1038/ncomms10437
- (39) Tian, B.; Wang, C.; Zhang, S.; Feng, L.; Liu, Z. Photothermally Enhanced Photodynamic Therapy Delivered by Nano-Graphene Oxide. *ACS Nano* **2011**, *5*, 7000–7009.
- (40) Zhang, C.; Bu, W.; Ni, D.; Zuo, C.; Cheng, C.; Li, Q.; Zhang, L.; Wang, Z.; Shi, J. A Polyoxometalate Cluster Paradigm with Self-Adaptive Electronic Structure for Acidity/Reducibility-Specific Photothermal Conversion. *J. Am. Chem. Soc.* **2016**, *138*, 8156–8164.
- (41) Hu, M.; Chen, J. Y.; Li, Z. Y.; Au, L.; Hartland, G. V.; Li, X. D.; Marquez, M.; Xia, Y. N. Gold Nanostructures: Engineering Their Plasmonic Properties for Biomedical Applications. *Chem. Soc. Rev.* **2006**, *35*, 1084–1094.
- (42) Chen, M.; Tang, S.; Guo, Z.; Wang, X.; Mo, S.; Huang, X.; Liu, G.; Zheng, N. Core-Shell Pd@Au Nanoplates as Theranostic Agents for *In-Vivo* Photoacoustic Imaging, CT Imaging, and Photothermal Therapy. *Adv. Mater.* **2014**, *26*, 8210–8216.
- (43) Song, X.; Chen, Q.; Liu, Z. Recent Advances in the Development of Organic Photothermal Nano-Agents. *Nano Res.* **2015**, *8*, 340–354.
- (44) Bardhan, R.; Chen, W.; Perez-Torres, C.; Bartels, M.; Huschka, R. M.; Zhao, L. L.; Morosan, E.; Pautler, R. G.; Joshi, A.; Halas, N. J. Nanoshells with Targeted Simultaneous Enhancement of Magnetic and Optical Imaging and Photothermal Therapeutic Response. *Adv. Funct. Mater.* **2009**, *19*, 3901–3909.
- (45) Liu, B.; Li, C.; Xing, B.; Yang, P.; Lin, J. Multifunctional UCNPs@PDA-ICG Nanocomposites for Upconversion Imaging and Combined Photothermal/Photodynamic Therapy with Enhanced Antitumor Efficacy. *J. Mater. Chem. B* **2016**, *4*, 4884–4894.
- (46) Kim, J.; Piao, Y.; Hyeon, T. Multifunctional Nanostructured Materials for Multimodal Imaging, and Simultaneous Imaging and Therapy. *Chem. Soc. Rev.* **2009**, *38*, 372–390.
- (47) Wang, S.; Li, X.; Chen, Y.; Cai, X.; Yao, H.; Gao, W.; Zheng, Y.; An, X.; Shi, J.; Chen, H. A Facile One-Pot Synthesis of a Two-Dimensional MoS₂/Bi₂S₃ Composite Theranostic Nanosystem for Multi-Modality Tumor Imaging and Therapy. *Adv. Mater.* **2015**, *27*, 2775–2782.
- (48) Stouwdam, J. W.; van Veggel, F. Improvement in the Luminescence Properties and Processability of LaF₃/Ln and LaPO₄/Ln Nanoparticles by Surface Modification. *Langmuir* **2004**, *20*, 11763–11771.
- (49) Liu, J.; Zheng, X.; Yan, L.; Zhou, L.; Tian, G.; Yin, W.; Wang, L.; Liu, Y.; Hu, Z.; Gu, Z.; Chen, C.; Zhao, Y. Bismuth Sulfide Nanorods as a Precision Nanomedicine for *in Vivo* Multimodal Imaging-Guided Photothermal Therapy of Tumor. *ACS Nano* **2015**, *9*, 696–707.
- (50) Liu, Z.; Ran, X.; Liu, J.; Du, Y.; Ren, J.; Qu, X. Non-Toxic Lead Sulfide Nanodots as Efficient Contrast Agents for Visualizing Gastrointestinal Tract. *Biomaterials* **2016**, *100*, 17–26.
- (51) Tian, Q.; Hu, J.; Zhu, Y.; Zou, R.; Chen, Z.; Yang, S.; Li, R.; Su, Q.; Han, Y.; Liu, X. Sub-10 nm Fe₃O₄@Cu_{2-x}S Core-Shell Nanoparticles for Dual-Modal Imaging and Photothermal Therapy. *J. Am. Chem. Soc.* **2013**, *135*, 8571–8577.
- (52) Tian, Q. W.; Tang, M. H.; Sun, Y. G.; Zou, R. J.; Chen, Z. G.; Zhu, M. F.; Yang, S. P.; Wang, J. L.; Wang, J. H.; Hu, J. Q. Hydrophilic Flower-Like CuS Superstructures as an Efficient 980 nm Laser-Driven Photothermal Agent for Ablation of Cancer Cells. *Adv. Mater.* **2011**, *23*, 3542–3547.
- (53) Zha, Z. B.; Wang, S. M.; Zhang, S. H.; Qu, E. Z.; Ke, H. T.; Wang, J. R.; Dai, Z. F. Targeted Delivery of CuS Nanoparticles Through Ultrasound Image-Guided Microbubble Destruction for Efficient Photothermal Therapy. *Nanoscale* **2013**, *5*, 3216–3219.
- (54) Meng, Z.; Wei, F.; Wang, R.; Xia, M.; Chen, Z.; Wang, H.; Zhu, M. NIR-Laser-Switched *in Vivo* Smart Nanocapsules for Synergic Photothermal and Chemotherapy of Tumors. *Adv. Mater.* **2016**, *28*, 245–253.
- (55) Zhou, M.; Zhang, R.; Huang, M.; Lu, W.; Song, S.; Melancon, M. P.; Tian, M.; Liang, D.; Li, C. A Chelator-Free Multifunctional [⁶⁴Cu]CuS Nanoparticle Platform for Simultaneous Micro-PET/CT

Imaging and Photothermal Ablation Therapy. *J. Am. Chem. Soc.* **2010**, *132*, 15351–15358.

(56) Li, Z. Q.; Zhang, Y. An Efficient and User-Friendly Method for the Synthesis of Hexagonal-Phase NaYF_4 : Yb, Er/Tm Nanocrystals with Controllable Shape and Upconversion Fluorescence. *Nanotechnology* **2008**, *19*, 345606. DOI: 10.1088/0957-4484/19/34/345606.